Cardiolipins are biomarkers of mitochondria-rich thyroid oncocytic tumors

Jialing Zhang[1], **Wendong Yu**[2], **Seung Ryu**[3], **John Lin**[1], **Gerardo Buentello**[4], **Robert Tibshirani**[5], **James Suliburk**[4,*], and **Livia S. Eberlin**[1,*]

[1]Department of Chemistry, The University of Texas at Austin, Austin, TX, 78712

[2]Department of Pathology and Immunology, Baylor College of Medicine, Houston, TX, 77030

[3]Department of Molecular Biosciences, The University of Texas at Austin, Austin, TX, 78712

[4]Department of Surgery, Baylor College of Medicine, Houston, TX, 77030

[5]Departments of Health Research and Policy and of Statistics, Stanford University, Stanford, CA 94305

Abstract

Oncocytic tumors are characterized by an excessive eosinophilic, granular cytoplasm due to aberrant accumulation of mitochondria. Mutations in mitochondrial DNA occurs in oncocytic thyroid tumors, but there is no information about their lipid composition which might reveal candidate theranostic molecules. Here we used desorption electrospray ionization mass spectrometry (DESI-MS) to image and chemically characterize the lipid composition of oncocytic thyroid tumors, as compared to non-oncocytic thyroid tumors and normal thyroid samples. We identified a novel molecular signature of oncocytic tumors characterized by an abnormally high abundance and chemical diversity of cardiolipins (CL), including many oxidized species. DESI-MS imaging and immunohistochemistry experiments confirmed that the spatial distribution of CL overlapped with regions of accumulation of mitochondria-rich oncocytic cells. Fluorescent imaging and mitochondrial isolation showed that both mitochondrial accumulation and alteration in CL composition of mitochondria occurred in oncocytic tumors cells, thus contributing the aberrant molecular signatures detected. A total of 219 molecular ions including CL, other glycerophospholipids (GP), fatty acids (FA), and metabolites were found at increased or decreased abundance in oncocytic, non-oncocytic or normal thyroid tissues. Our findings suggest new candidate targets for clinical and therapeutic use against oncocytic tumors.

Keywords

mass spectrometry imaging; cardiolipin; mitochondria; oncocytic tumors; ambient ionization

---

[*]to whom correspondence should be addressed: suliburk@bcm.edu and liviase@utexas.edu.

Introduction

Oncocytic tumors are a distinctive class of proliferative lesions composed of cells with an aberrant accumulation of mitochondria (1). Tumors composed of oncocytic cells are particularly common among thyroid neoplasms of follicular cell derivation. Clinically, oncocytic thyroid tumors (also called Hurthle cell neoplasms) have poorer oncologic outcomes than their non-oncocytic counterparts, and are thus considered an adverse prognostic indicator. The biological mechanisms underlying mitochondria accumulation in oncocytic tumors are not fully understood. Sequencing studies have reported up-regulation of genes involved in mitochondrial biogenesis and oxidative metabolism in thyroid oncocytic tumors, including genes from the tricarboxylic acid cycle and cytosolic glycolysis (2). More recently, mutations in the mtDNA disruptive complex I have been described as potential markers of oncocytic lesions (3).

The inner mitochondrial membrane of eukaryotic cells has a complex structure and molecular composition, recognized by the presence of cardiolipins (CL), a unique class of anionic GP located predominantly (if not exclusively) in mitochondria. CL have a distinctive chemical structure, composed of two phosphatidylglycerols bridged via a glycerol backbone, which displays two negative charges from the phosphate groups and four acyl chains. These complex lipids play multiple structural and functional roles in bioenergetics, mitochondrial signaling, cellular fate pathways, and are associated with individual complexes of the electron transport. Dysregulation of CL expression and composition has been increasingly investigated in biological samples using high-performance liquid chromatography mass spectrometry (HPLC-MS). Lipid analysis by HPLC-MS provides rich and quantitative information from biological samples. Yet, these time-consuming assays require sample homogenization, and thus disregard cellular heterogeneity within biological tissue samples and preclude acquisition of spatial information. Recently, HPLC-MS was used to identify CL and oxidized CL species in a rat model of traumatic brain injury (4). CL were also identified by HPLC-MS as proliferation markers in prostate cancer cell lines, and differences in CL composition were seen in tissues from six prostate cancer patients, although with no statistical significance (5). In clinical research, the ratio of the intensities of CL and monolysocardiolipins (MLCL), measured in blood by HPLC-MS, has been suggested as a screening test for Barth Syndrome (6). Despite the importance of CL in physiological function and its role in mediating the pathology of disease states, no studies have investigated their role in human thyroid tumor tissues.

Here, we used mass spectrometry imaging to chemically characterize the lipid signatures of thyroid tumors. We discovered a rich molecular signature uniquely characterized by a high abundance and diversity of CL species in oncocytic thyroid tumors. Different CL species including oxidized cardiolipins (ox-CL), adducts of CL and glycerophosphocholines (PC) or diacylglycerides (DG), and MLCL were identified at high relative abundances in oncocytic tumors when compared to non-oncocytic tumors and normal thyroid tissues. DESI-MS imaging and optical imaging of stained tissues, even though in a different spatial scale, confirmed that the CL distribution and highest intensity co-localized with regions of oncocytic tumor cells in thyroid tissues. Fluorescent imaging and mitochondrial isolation studies showed that mitochondrial accumulation and alteration in CL composition of

mitochondria occur in oncocytic tumors cells, thus contributing the aberrant molecular signatures detected. Statistical analysis showed that CL species were increased in oncocytic tumors with the highest statistical significance, while other GP and FA were also found to significantly discriminate oncocytic tumors, non-oncocytic tumors, and normal thyroid tissues.

MS imaging has been extensively used to investigate the lipid profiles of human tumors (7,8). In particular, ambient ionization MS imaging techniques such as DESI-MS allow for direct analysis of tissue sections, in the open air environment, and with minimal sample preparation (9–12). DESI-MS has been used to characterize the lipid profiles of brain (13,14), gastric (15), breast (16,17), and other cancers (18). Variations in the relative and total abundances of FA and most abundant complex lipids classes have been described in cancer tissues when compared to normal tissues (18). Yet, as the abundance of CL in cells and tissues is low relative to other lipids, little has been reported on the changes of CL in cancer tissue using MS imaging. Matrix-assisted laser desorption/ionization mass spectrometry (MALDI-MS) has been employed to analyze CL in animal model tissues or cell lines (19–21). Using DESI-MS imaging, five different CL species were identified in MYC-induced lymphoma mice tissue (22), and a single CL specie was detected in normal human gastric epithelial tissue (15). To the best of our knowledge, this is the first study to report a diverse group of CL species as molecular markers of human tumors. As lipid signatures can be readily accessed using ambient MS imaging, we expect this method to be valuable for clinical use (18).

Materials and Methods

For detailed information on materials and methods, please see Supporting Information.

Banked Human Thyroid Tissues

A total of 45 frozen human thyroid tissue specimens were obtained from Cooperative Human Tissue Network, Baylor College Tissue Bank, and Asterand Biosciences under approved IRB protocol. A first set of 30 samples included 10 oncocytic thyroid tumors (8 hurthle cell adenomas and 2 hurthle cell carcinomas), 10 non-oncocytic thyroid tumors (5 papillary thyroid carcinomas and 5 follicular thyroid adenoma) and 10 normal thyroid tissues. A second set was purchased and analyzed independently including 5 oncocytic thyroid tumors (2 hurthle cell adenomas and 3 hurthle cell carcinomas), and 10 non-oncocytic thyroid tumors (5 papillary thyroid carcinomas and 5 follicular thyroid carcinomas). All tissue samples were sectioned at 16 μm thick sections, and stored in a −80°C freezer until analysis.

DESI-MS imaging

A 2D Omni Spray (Prosolia Inc., Indianapolis, IN) was used for tissue imaging with a spatial resolution of 150 μm. DESI-MS imaging was performed in the negative ion mode from m/z 100–1500, using a hybrid LTQ-Orbitrap Elite mass spectrometer (Thermo Scientific, San Jose, CA). The histologically compatible solvent system dimethylformamide:acetonitrile 1:1 was used for analysis (23). For ion identification, high

mass resolution/accuracy measurements and tandem MS analyses were performed in the Orbitrap and the linear ion trap using the same tissue sections analyzed.

Histopathology

The same tissue sections analyzed by DESI-MSI were subjected afterwards to H&E staining. Pathologic evaluation was performed by Dr. Wendong Yu using light microscopy. Regions of clear diagnosis of cancer and normal thyroid tissue were assigned in the glass slides.

Immunohistochemistry, Immunofluorescence and Confocal Microscopy

For immunohistrochemistry, formalin fixed tissue sections were stained for human mitochondria using primary Human Mitochondria monoclonal antibody MAB1273 (Millipore, Billerica, MA). All the H&E and IHC stained slides were scanned by using the Aperio ScanScope imaging platform (Aperio Technologies, Vista, CA) with a 20x objective at a spatial sampling period of 0.47 μm per pixel. Whole slides images (WSI) were viewed and analyzed by using desktop personal computers equipped with the free ScanScope software. For immunofluorescence, formalin fixed tissues were stained using Alexa Fluor 488 conjugated anti-mitochondrial antibody MAB1273A4 (Millipore, Billerica, MA), counterstained and mounted in ProLong Gold Antifade mounting media (Thermo Fisher). Immunofluorescence images were acquired on a Zeiss LSM880 confocal microscope.

Mitochondria isolation and analysis

Mitochondria isolation was carried out following a organelle isolation protocol (24). Quantification was done using BCA Protein Assays kit (Thermo scientific, Austin, TX). Concentrations were measured by comparing absorbance to standard protein calibration curve created with different concentration of BSA. Total lipid extraction was carried out by Bligh-Dyer method.

Statistical Analysis

Regions of interest in the 2D raw data obtained by DESI-MSI were selected, converted to text files, and imported to R language for statistical analysis using the SAM method.

Results

Molecular characterization of cardiolipins in oncocytic tissue

Negative ion mode DESI-MS was used to analyze a total of 45 human thyroid samples, including 15 oncocytic thyroid tumors (10 hurthle cell adenomas and 5 hurthle cell carcinomas), 20 non-oncocytic thyroid tumors (10 papillary thyroid carcinomas, 5 follicular carcinomas, and 5 follicular thyroid adenoma) and 10 normal thyroid tissues. The mass spectra obtained from m/z 100–1500 (Supporting Figure 1) presented high relative abundances of several molecular ions commonly characterized as lipid species in the negative ion mode DESI mass spectra of human tissues, including FA and GP such as glycerophosphoinositols (PI), glycerophosphoethanolamines (PE), and glycerophosphoserines (PS). Normal thyroid tissue displayed high relative abundances of PI

(20:4/18:0) (m/z 885.548), PS (20:3/18:0) (m/z 812.544), PS (18:1/18:0) (m/z 788.544), PE (20:4/18:0) (m/z 766.538), PE (18:2/18:1) (m/z 742.538) and phosphatidic acids (PA) (18:1/18:0) (m/z 701.512) which are lipid ions commonly detected from mammalian tissues (Figure 1, bottom panel). In contrast, the mass spectra obtained from oncocytic tumor samples showed a very distinct and reproducible profile with abnormally high relative abundances of a series of doubly charged ions in the mass range from m/z 590–760, and m/z 1000–1200 (Figure 1, top panel). The spectra were remarkably rich in molecular diversity, and unlike what commonly observed in human cancer tissues by DESI-MS imaging. It should be noted that ions with two negative charges are characterized by a mass-to-charge ratio (m/z) corresponding to half the molecular weight of the ion. Doubly charged ions are easily recognized by MS as the ^{13}C isotope peak is at a 0.5 m/z difference from the ^{12}C isotope peak (Figure 1, inset on top panel), while for singly charged ions the ^{13}C peak is observed with 1 m/z difference. Doubly charged lipid ions are unusually detected at high intensities from human tissues by DESI-MS analysis, and stand out from other FA and GP ions which are most commonly observed as singly charged species in the negative ion mode.

Using high mass accuracy measurements and tandem MS analysis via collision-induced dissociation (CID) and higher-energy collisional dissociation (HCD), we identified these doubly charged ions as a diverse group of CL species. Structural elucidation using lithium adducts was also explored and provided confirmatory structural information (Supporting Figure 2) (25). CL have been previously investigated by electrospray ionization and tandem MS and present key fragment ions that enable structural characterization (26–28). For example, tandem MS experiments of doubly charged molecular ion m/z 724.483 yielded fragment ions corresponding to 18:2-carboxylate anion (m/z 279.233), 18:1-carboxylate anion (m/z 281.249), 20:2-carboxylate anion (m/z 307.264), lyso-PA fragments (m/z 415.225, m/z 417.241 and m/z 461.249), a doubly charged ketene (m/z 593.371) arising from loss of the 18:2-fatty acyl substituent, and a fragment ion at m/z 1169.737 produced by neutral loss of FA(18:2), indicating that the molecular ions corresponds to CL(20:2/18:2/18:1/16:2 or 18:2/18:2/18:2/18:1) (Supporting Figure 3). High mass accuracy measurements agrees with the exact mass (m/z 724.4867) of proposed molecular formula ($C_{81}H_{144}O_{17}P_2$) with a mass error of −1.7 ppm. Note that isomerism of the double bonds in the fatty acid (FA) chains of GP complicates precise structural assignment, which is why acyl chains are only tentatively assigned. Furthermore, several combinations of the four acyl chains at different positions in the CL structure are possible, thus, the exact configuration cannot be assigned by our method. In total, 31 CL molecular ions were identified and characterized, except for two CL ions which present insufficient fragment ions intensity. The singly charged CL molecular ions were also observed from m/z 1400–1500 at high relative intensities in the oncocytic tumor when compared to non-oncocytic and normal thyroid tissues.

Several ox-CL species were also identified in the oncocytic tumors mass spectra. For example, tandem MS experiments of doubly charged molecular ion m/z 677.414 yielded oxidized carboxylate anion (9:1-OOH) (m/z 187.099), 18:2-carboxylate anion (m/z 279.234), oxidized lyso-PA from (9:1-OOH) at m/z 323.092, and lyso-PA at m/z 415.228, indicating that the CL molecular species is ox-CL(18:2/18:2/18:2/9:1(OOH)) (Supporting Figure 3) (29). Altogether, 17 different ox-CLs were identified in oncocytic tumor tissues,

previously unreported in human tissues. Note that these oxidized species were also observed in oncocytic tissues when no voltage was applied in the DESI source (30). Most interestingly, this oxidation effect was specific to CL, as other polyunsaturated GP at similar relative abundances were not detected in their oxidized forms by our method. Thus, our data indicates that the detected ox-CL are endogenous molecules present in oncocytic tissues.

An uncommon series of doubly charged peaks from m/z 1000–1200 were observed in high relative abundance in oncocytic tumors when compared to non-oncocytic and normal thyroid tissues. These peaks were identified using a series of tandem MS experiments as a combination of CL with DG (m/z 1000–1100), or, more predominantly observed, with PC (m/z 1100–1200), with no bridging or other additional atoms. The ion m/z 1102.262, for example, was identified as CL+PC (106:12) using MS^2 and MS^3 experiments (Supporting Figure 3). The chemical structure of many fragment ions include structural components of both PC and CL molecules, which indicates that these species are strongly bound, through what we hypothesize to be an ionic bond within a concatenated structure. To confirm the chemical composition of these ions, we performed DESI-MS analysis on a mixture of CL and PC standards, and observed the formation of these doubly charged species which presented identical fragmentation pattern (Supporting Figure 4) to those observed in tissue. PC were not observed in negative ion mode in our experiments, thus, it is interesting to observe these molecules bound to CL species. We have not found previous reports on the observations of these doubly charged molecular ions from tissue samples.

In total, 28 CL species, 17 ox-CL, 2 MLCL, 27 CL+PC, and 27 CL+DG were identified in oncocytic tumors. The results for a representative set of these species are shown in Table 1, while the full list is can be found in Supporting Table 1 (note that only C^{12} isotope was included for each molecule). Note that two MLCL species were identified in oncocytic thyroid tumor tissue, although at a lower relative intensity when compared to the other CL species detected. In contrast to oncocytic thyroid tumors, the mass spectra obtained from non-oncocytic thyroid tumors showed high relative abundances of PI(20:4/17:0) at m/z 871.536, PI(20:4/16:0) at m/z 857.520, PI(18:2/16:0) at m/z 833.518, and PE(18:1/O-16:1) at m/z 700.530 (Figure 1), as well as many other GP and FA. CL species were also observed in non-oncocytic tumors but at lower relative intensities than what observed in oncocytic thyroid tumors, while oxidized species were either undetectable or at much lower abundance using our method. In normal thyroid tissues, while the mass spectra total ion counts were similar to those observed from tumor tissues, all ox-CL species identified in oncocytic tissues were undetectable by DESI-MS (Supporting Figure 5). While the DESI-MS imaging results provide a qualitative assessment of the changes in lipid abundances, multivariate statistical analysis of the individual ions was performed to evaluate if the observed changes are significant (results shown later in the manuscript).

Cardiolipin distribution correlates with oncocytic cells and mitochondria accumulation in tissues

2D DESI-MSI experiments were performed to examine the spatial distribution of the molecular ions detected from thyroid tissues (Figure 2A). In particular, we were interested to investigate if the spatial distribution of CL ions co-localized with specific histological

features in oncocytic tumor tissues. Figure 2B shows the DESI-MS images obtained for selected molecular ions for an oncocytic sample, a non-oncocytic sample, and normal thyroid tissue sample (additional imaging results are shown in Supporting Figure 6). Optical images of the same tissue section which were H&E stained after DESI-MSI are also presented (23). On a microscopic scale, all oncocytic tumors analyzed showed characteristic histological features with enlarged cells of high cytoplasmic volume that accommodates the increased number of mitochondria. In many samples, regions predominantly composed of cancer cells were observed adjacent or within regions defined as regions of fibrosis tissues. These tissue regions (hundreds of micrometers) were spatially assigned by pathologic evaluation and were discernable in the DESI-MS images (spatial resolution of 150 μm). In oncocytic tumors, the molecular distribution of CL species was co-localized, homogeneous, and remarkably high within the regions of oncocytic tumor cells and were in lower intensities in fibrosis regions in sample, as shown for m/z 738.502 and m/z 723.479 (Figure 2B). Similar spatial distribution was observed for other CL, ox-CL, CL+PC, and CL+DG molecular ions (Figure 3). In particular, all ox-CL showed highly similar spatial distributions with increased relative intensities observed in regions with accumulation of oncocytic thyroid tumor cells and absence in adjacent normal cells or fibrosis. In all normal thyroid tissue analyzed, common patterns of the cellular organization were observed, with spherical colloid surrounded by a single layer of follicular cells and scattered parafollicular cells. The molecular images obtained for normal tissues showed lipid signal co-localized with follicular cells (Figure 2B). Colloid did not show lipid profiles and are thus seen as dark regions in the DESI-MS ion images. Non-oncocytic follicular and papillary thyroid carcinoma showed typical histological patterns, and displayed a homogenous molecular distribution of the most abundant molecular ions within regions of tumor cell.

To evaluate if CL distribution correlates with regions of mitochondrial accumulation in oncocytic tumors, we performed immunohistochemistry (IHC) with an anti-mitochondrial antibody in tissues sections adjacent to those imaged by DESI-MS. Positive staining for mitochondria was observed for all thyroid tumors analyzed, while negative (weak) staining was observed for all normal thyroid tissues. As expected, strong mitochondrial staining are seen in all oncocytic tissues (Supporting Figure 7). Spatial agreement was observed between regions of strong mitochondrial staining in oncocytic tissues and regions of high relative intensities of CL species in DESI-MS images. Papillary thyroid carcinoma that presented higher relative abundances of CL also showed mitochondria staining by IHC.

Mitochondria accumulates in oncocytic thyroid tumor cells

To further investigate the mitochondrial distribution within the cells of thyroid tissues, we performed immunofluorescence staining with an anti-mitochondrial antibody (green) and nuclear staining (blue) in adjacent sections of thyroid tissues (Figure 4A). Confocal microscopy images obtained for oncocytic tumors show high density staining of mitochondria. A punctate staining pattern showcases accumulation of mitochondria within the cellular cytoplasm in oncocytic tumors. Non-oncocytic follicular carcinoma shows less pronounced accumulation of mitochondria in scattered cell, lower than what observed for oncocytic tumors, and significantly higher than normal tissue. To provide a quantitative assessment of mitochondrial in thyroid tissue, tissues were homogenized and mitochondria

was isolated following a specific organelle isolation protocol (Figure 2A) (24). Quantification of the total protein content in the isolated mitochondria pallet by UV-Vis shows that there is on average 2.5 times more protein present in the mitochondrial fraction of oncocytic tumor tissues when compared to normal thyroid tissues. Normal thyroid samples contained on average 8.8 mg of protein/g of tissue sample, while oncocytic tumor samples contained 22.2 mg of protein/g of tissue sample and non-oncocytic thyroid tumors contained 15.6 mg of protein/g of tissue sample (Figure 4B). The changes in mitochondrial protein content between groups were found to be statistically significantly (p value<0.001 using a one-way analysis of variance test).

Alteration in CL composition occurs in the mitochondria of oncocytic human tumor cells

We questioned rather the abnormally high relative abundances of and diversity of CL species detected from oncocytic tissues were solely related to accumulation of mitochondria per oncocytic cell, or also associated to an alteration in the CL composition of the mitochondria membrane. To investigate this question, we diluted the isolated mitochondrial pallets to the same concentration (3 μg protein/g of tissue) for all tissues, performed a lipid extraction, and analyzed using the same conditions used for DESI-MS imaging of tissue sections. The mass spectra obtained showed a higher relative intensity of CL species from the mitochondria isolated from oncocytic tumors when compared to non-oncocytic tumors and normal thyroid tissues (Supporting Figure 8). To compare the CL abundance within the samples, we normalized the total ion counts of CL species to the total lipid counts in the spectra obtained from isolated mitochondria. The average normalized value was 0.081 for oncocytic tumors, 0.037 for non-oncocytic tumors, and 0.002 for normal tissue (Figure 4C), which allows discrimination between these groups with statistical significance (p value<0.001 using a one-way analysis of variance test). These results confirm that besides mitochondria accumulation, an alteration in the CL composition of the mitochondrial membrane occurs in oncocytic thyroid cells. These biological phenomena collectively contribute to the abnormally high relative intensities and diversity of CL species detected directly from oncocytic tumor tissue in our DESI-MS imaging experiments.

Lipids are molecular markers of oncocytic tumors

To evaluate if the changes in relative abundances of the molecular ions observed in DESI mass spectra and images obtained were statistically significant, we applied significance analysis of microarrays (SAM) statistical analysis to our complex DESI-MS imaging dataset. Mass spectral data were extracted from regions of interest of a single predominant histological composition for the first set of 30 samples investigated (i.e. cancer cells, or normal follicular cells). SAM identifies if the change in the abundance of a molecular ion (*m/z* value) is statistically significant between the three different phenotypes by computing a contrast value that measures the average change in the peak intensity for that *m/z* between the groups.(31) Repeated permutations were used to determine whether the change is significantly related to the phenotype and to estimate the percentage of molecular ions identified by chance, the false discovery rate (FDR). The mean intensity value for all samples for a certain *m/z* was set to zero, so that the contrast values obtained represent the mean fold increase (positive contrast) or decrease (negative contrast) for the groups when compared to the overall mean intensity value. From all the ions detected (*m/z* 100 – 1500)

for all the samples analyzed, 219 different molecular ions were selected with FDR< 5%. As expected, ions corresponding to MLCL, ox-CL, CLs, CL+PC and CL+DG presented the most significant changes in average abundances between the three groups by SAM analysis. For example, the singly charged CL (20:4/18:2/18:2/16:0 or 18:2/18:2/18:2/18:2) detected at *m/z* 1447.975 presented the highest contrast values of −1.927 for normal tissue, −0.845 for non-oncocytic tumors, and +2.772 for oncocytic tumors (FDR=0). Figure 5A shows the overall trend in contrast values obtained for the cardiolipin species selected by SAM (FDR<5%). As observed, all CL species present positive values for oncocytic tumors, which demonstrates that these lipids are significant for discriminating oncocytic tumors from non-oncocytic tumors and normal thyroid tissues. Box plots for selected ions are shown in Figure 5B. Highly reproducible results which corroborates these findings were obtained in a set of 15 independent thyroid tumors analyzed (Supporting Figure 9). The remaining GP selected by SAM (FDR<5%) including PI, PE and PG presented no clear trends in contrast values within the three groups.

Discussion

Accumulation of cardiolipin-rich mitochondria is a fundamental characteristic of oncocytic tumors. Mutations in mitochondrial DNA have been previously described in oncocytic thyroid tumors, yet, little is known on their lipid composition. In this study, we used DESI-MS to image and chemically characterize the lipid composition of thyroid tumors. We discovered a novel molecular signature in oncocytic tumors characterized by an abnormally high abundance and chemical diversity of CL species. DESI-MS imaging and IHC experiments confirmed that the spatial distribution of these molecular ions overlapped with regions of accumulation of mitochondria-rich oncocytic cells. Fluorescence imaging confirmed that the oncocytic tumors investigated presented high accumulation of mitochondria when compared to non-oncocytic and normal thyroid tissue.

Using high-mass accuracy, high-mass resolution, and tandem MS experiments, we identified 101 different CL-containing molecular ions directly from oncocytic thyroid tissues. MS imaging of this large amount and diversity of CL species is unprecedented in untreated human tissues. Amongst these, two MLCL, which are intermediates molecules in CL remodeling (32), were detected in oncocytic thyroid tumor tissues. In addition, 54 intriguing doubly charged molecular ions composed of CL bound to PC or DG were seen at high relative abundances in oncocytic tumors when compared to non-oncocytic or normal thyroid tissues. The mitochondrial inner membrane of eukaryotic cells has a unique composition of GP, predominantly composed of PC, CL, and PE, although the exact percent composition of lipids in human mitochondria is not known (33). Thus, the detection of CL+PC molecular ions, while unexpected, is not surprising considering the composition and spatial proximity of these molecules in the inner mitochondria membrane of oncocytic tumors.

Remarkably, we identified 17 different ox-CL in oncocytic tumors. Oxidization of other abundant polyunsaturated phospholipids were not observed in our experiments, which indicates that this phenomena is primarily occurring for CL, likely due to mitochondria dysregulation which is known to occur in oncocytic thyroid tumors (2). CL oxidation have been implicated in degenerative diseases and reported in neuronal tissue that has suffered

traumatic brain injury (4). Oxidative stress has been largely connected to tumorigenesis. In the mitochondrial inner membrane, CL are found in association with the components of the electron transport chain (ETC), which generates reactive oxygen species. The proximity of the FA chains of CL to the various ETC complexes make it a likely target of oxidative damage (29). Furthermore, redistribution of mitochondrial membrane CL and accumulation of CL oxidation products through interactions with cytochrome c are required stages in the cellular apoptotic program, a process known to occur in tumor progression (34). Recently, ox-CL were detected in PC-3 prostate cancer cell lines although their content did not correlate with the proliferation of cells (5). We have also detected ox-CL in human kidney oncocytic tumors (unpublished), further suggesting their importance in oncocytic neoplasms although more rigorous studies are needed to determine their biological role in human tumors.

This is the first study to report abnormal expression and composition of lipids such as CL in human thyroid tumor tissues. Through immunofluorescence imaging, DESI-MS imaging, and mitochondria isolation experiments, we demonstrated that this aberrant CL signature are related to: 1. Accumulation of mitochondria in oncocytic tumors, and 2. Dysregulation (increased abundance and diversified structures) of CL composition in mitochondria membrane of oncocytic tumor cells. Gene expression profiling studies have suggested a profound modification of energy metabolism in oncocytic tumors (2). Genes coding for subunits of the respiratory chain enzymes, glycolytic enzymes, and energy metabolism enzymes involved in glycolysis, the tricarboxylic acid cycle are overexpressed in oncocytic tumors, many of which are directly involved in lipid biogenesis and metabolism. Our results further suggest that dysregulation of mitochondria and lipid metabolism is relevant in oncocytic tumors, and provide novel molecular information for deciphering the biological mechanisms involved in these tumors.

The thyroid is the main hormonal regulator of lipid biogenesis and mitochondrial function (35). Nevertheless, no previous studies have investigated the lipid signatures of thyroid tumors. We show that lipids are molecular markers of oncocytic tumors with statistical significance. While direct MS imaging does not provide a quantitative assessment of molecules in tissues, using SAM, 219 distinct molecular ions (FDR<5%) including various lipids and metabolites were found at increased or decreased relative abundance in oncocytic, non-oncocytic or normal thyroid tissues. Besides CL, significant changes in FA abundances were also observed using statistical analysis. This rich lipid signature is characteristic and diagnostic of oncocytic phenotypes. Although our sample size is not sufficient for discriminating adenomas and carcinomas within the oncocytic tumor group, our pilot study gives further rational to explore this problem using the molecular information obtained by ambient ionization MS. Importantly, these unprecedented findings provide possibilities for new therapeutic targets for oncocytic tumors.

As lipid signatures can be readily accessed from tissue samples using ambient ionization MS, we expect this method to be valuable for diagnosis of thyroid cancers and clinical use (18). Nondestructive DESI-MS can be adapted for fine needle aspiration biopsy analysis, the gold standard method for pre-operative diagnosis of thyroid lesions. With further increase in sample size and analysis of different tumor types, we expect to identify unique molecular

signatures in various types of thyroid neoplasia in order to enhance diagnosis of nodules (especially those deemed indeterminate) and thus overcome current limitations of thyroid cytology.

Our work showcases the power of ambient ionization MS for CL imaging in biological tissues and is relevant to a variety of applications. Dysregulation of mitochondria occurs in many pathologies besides cancer. Lipids and their oxidized counterparts have been increasingly appreciated as important molecular markers and investigated to uncover biological pathways in disease (36–38). Further studies will be performed to extensively investigate alterations in small metabolites, FA, CL, and other GP in thyroid tumors.

Supplementary Material

Refer to Web version on PubMed Central for supplementary material.

Acknowledgments

References

1. Tallini G. Oncocytic tumours. Virchows Archiv-an International Journal of Pathology. 1998; 433(1): 5–12. [PubMed: 9692819]

2. Baris O, Savagner F, Nasser V, Loriod B, Granjeaud S, Guyetant S, et al. Transcriptional profiling reveals coordinated up-regulation of oxidative metabolism genes in thyroid oncocytic tumors. Journal of Clinical Endocrinology & Metabolism. 2004; 89(2):994–1005. [PubMed: 14764826]

3. Gasparre G, Porcelli AM, Bonora E, Pennisi LF, Toller M, Iommarini L, et al. Disruptive mitochondrial DNA mutations in complex I subunits are markers of oncocytic phenotype in thyroid tumors. Proceedings of the National Academy of Sciences of the United States of America. 2007; 104(21):9001–06. [PubMed: 17517629]

4. Ji J, Kline AE, Amoscato A, Samhan-Arias AK, Sparvero LJ, Tyurin VA, et al. Lipidomics identifies cardiolipin oxidation as a mitochondrial target for redox therapy of brain injury. Nature Neuroscience. 2012; 15(10):1407–13. [PubMed: 22922784]

5. Sapandowski A, Stope M, Evert K, Evert M, Zimmermann U, Peter D, et al. Cardiolipin composition correlates with prostate cancer cell proliferation. Molecular and Cellular Biochemistry. 2015; 410(1–2):175–85. [PubMed: 26314254]

6. Corcelli A, Angelini R, Lobasso S, Bowron A, Steward C. Monolysocardiolipin/cardiolipin ratio of intact leukocytes as novel tool for the screening of Barth Syndrome. Faseb Journal. 2015;29.

7. Norris JL, Caprioli RM. Analysis of Tissue Specimens by Matrix-Assisted Laser Desorption/Ionization Imaging Mass Spectrometry in Biological and Clinical Research. Chemical Reviews. 2013; 113(4):2309–42. [PubMed: 23394164]

8. Wu C, Dill AL, Eberlin LS, Cooks RG, Ifa DR. Mass spectrometry imaging under ambient conditions. Mass Spectrometry Reviews. 2013; 32(3):218–43. [PubMed: 22996621]

9. Wiseman JM, Ifa DR, Song QY, Cooks RG. Tissue imaging at atmospheric pressure using desorption electrospray ionization (DESI) mass spectrometry. Angew Chem-Int Ed. 2006; 45(43): 7188–92.

10. Takats Z, Wiseman JM, Gologan B, Cooks RG. Mass spectrometry sampling under ambient conditions with desorption electrospray ionization. Science. 2004; 306(5695):471–73. [PubMed: 15486296]

11. Hsu C-C, Dorrestein PC. Visualizing life with ambient mass spectrometry. Current Opinion in Biotechnology. 2015; 31:24–34. [PubMed: 25146170]

12. Nemes P, Vertes A. Ambient mass spectrometry for in vivo local analysis and in situ molecular tissue imaging. Trac-Trends in Analytical Chemistry. 2012; 34:22–34.

13. Jarmusch AK, Pirro V, Baird Z, Hattab EM, Cohen-Gadol AA, Cooks RG. Lipid and metabolite profiles of human brain tumors by desorption electrospray ionization-MS. Proceedings of the National Academy of Sciences of the United States of America. 2016; 113(6):1486–91. [PubMed: 26787885]

14. Eberlin LS, Norton I, Dill AL, Golby AJ, Ligon KL, Santagata S, et al. Classifying Human Brain Tumors by Lipid Imaging with Mass Spectrometry. Cancer Research. 2012; 72(3):645–54. [PubMed: 22139378]

15. Eberlin LS, Tibshirani RJ, Zhang JL, Longacre TA, Berry GJ, Bingham DB, et al. Molecular assessment of surgical-resection margins of gastric cancer by mass-spectrometric imaging. Proceedings of the National Academy of Sciences of the United States of America. 2014; 111(7): 2436–41. [PubMed: 24550265]

16. Calligaris D, Caragacianu D, Liu X, Norton I, Thompson CJ, Richardson AL, et al. Application of desorption electrospray ionization mass spectrometry imaging in breast cancer margin analysis. Proceedings of the National Academy of Sciences of the United States of America. 2014; 111(42): 15184–89. [PubMed: 25246570]

17. Guenther S, Muirhead LJ, Speller AVM, Golf O, Strittmatter N, Ramakrishnan R, et al. Spatially Resolved Metabolic Phenotyping of Breast Cancer by Desorption Electrospray Ionization Mass Spectrometry. Cancer Research. 2015; 75(9):1828–37. [PubMed: 25691458]

18. Ifa DR, Eberlin LS. Ambient Ionization Mass Spectrometry for Cancer Diagnosis and Surgical Margin Evaluation. Clinical Chemistry. 2016; 62(1):111–23. [PubMed: 26555455]

19. Amoscato AA, Sparvero LJ, He RR, Watkins S, Bayir H, Kagan VE. Imaging Mass Spectrometry of Diversified Cardiolipin Molecular Species in the Brain. Analytical Chemistry. 2014; 86(13): 6587–95. [PubMed: 24949523]

20. Angelini R, Lobasso S, Gorgoglione R, Bowron A, Steward CG, Corcelli A. Cardiolipin fingerprinting of leukocytes by MALDI-TOF/MS as a screening tool for Barth syndrome. Journal of Lipid Research. 2015; 56(9):1787–94. [PubMed: 26144817]

21. Sparvero LJ, Amoscato AA, Kochanek PM, Pitt BR, Kagan VE, Bayir H. Mass-spectrometry based oxidative lipidomics and lipid imaging: applications in traumatic brain injury. Journal of Neurochemistry. 2010; 115(6):1322–36. [PubMed: 20950335]

22. Eberlin LS, Gabay M, Fan AC, Gouw AM, Tibshirani RJ, Felsher DW, et al. Alteration of the lipid profile in lymphomas induced by MYC overexpression. Proceedings of the National Academy of Sciences of the United States of America. 2014; 111(29):10450–55. [PubMed: 24994904]

23. Eberlin LS, Ferreira CR, Dill AL, Ifa DR, Cheng L, Cooks RG. Non-Destructive, Histologically Compatible Tissue Imaging by Desorption Electrospray Ionization Mass Spectrometry. ChemBioChem. 2011; 12(14):2129–32. [PubMed: 21793152]

24. Frezza C, Cipolat S, Scorrano L. Organelle isolation: functional mitochondria from mouse liver, muscle and cultured filroblasts. Nature Protocols. 2007; 2(2):287–95. [PubMed: 17406588]

25. Hsu FF, Bohrer A, Turk J. Formation of lithiated adducts of glycerophosphocholine lipids facilitates their identification by electrospray ionization tandem mass spectrometry. Journal of the American Society for Mass Spectrometry. 1998; 9(5):516–26. [PubMed: 9879366]

26. Hsu FF, Turk J, Rhoades ER, Russell DG, Shi YX, Groisman EA. Structural characterization of cardiolipin by tandem quadrupole and multiple-stage quadrupole ion-trap mass spectrometry with electrospray ionization. Journal of the American Society for Mass Spectrometry. 2005; 16(4):491–504. [PubMed: 15792718]

27. Han XL, Yang K, Yang JY, Cheng H, Gross RW. Shotgun lipidomics of cardiolipin molecular species in lipid extracts of biological samples. Journal of Lipid Research. 2006; 47(4):864–79. [PubMed: 16449763]

28. Kiebish MA, Han XL, Cheng H, Chuang JH, Seyfried TN. Cardiolipin and electron transport chain abnormalities in mouse brain tumor mitochondria: lipidomic evidence supporting the Warburg theory of cancer. Journal of Lipid Research. 2008; 49(12):2545–56. [PubMed: 18703489]

29. Kim J, Minkler PE, Salomon RG, Anderson VE, Hoppel CL. Cardiolipin: characterization of distinct oxidized molecular species. Journal of Lipid Research. 2011; 52(1):125–35. [PubMed: 20858593]

30. Pasilis SP, Kertesz V, Van Berkel GJ. Unexpected analyte oxidation during desorption electrospray ionization-mass spectrometry. Analytical Chemistry. 2008; 80(4):1208–14. [PubMed: 18183963]

31. Storey JD, Tibshirani R. Statistical significance for genomewide studies. Proceedings of the National Academy of Sciences of the United States of America. 2003; 100(16):9440–45. [PubMed: 12883005]

32. Tyurina YY, Poloyac SM, Tyurin VA, Kapralov AA, Jiang JF, Anthonymuthu TS, et al. A mitochondrial pathway for biosynthesis of lipid mediators. Nature Chemistry. 2014; 6(6):542–52.

33. Gohil VM, Greenberg ML. Mitochondrial membrane biogenesis: phospholipids and proteins go hand in hand. Journal of Cell Biology. 2009; 184(4):468–72.

34. Kagan VE, Tyurin VA, Jiang JF, Tyurina YY, Ritov VB, Amoscato AA, et al. Cytochrome c acts as a cardiolipin oxygenase required for release of proapoptotic factors. Nature Chemical Biology. 2005; 1(4):223–32. [PubMed: 16408039]

35. Hoch FL. LIPIDS AND THYROID-HORMONES. Progress in Lipid Research. 1988; 27(3):199–270. [PubMed: 3075762]

36. Camarda R, Zhou AY, Kohnz RA, Balakrishnan S, Mahieu C, Anderton B, et al. Inhibition of fatty acid oxidation as a therapy for MYC-overexpressing triple-negative breast cancer. Nature Medicine. 2016; 22(4):427–32.

37. Gross RW, Han X. Lipidomics at the interface of Structure and Function in Systems Biology. Chemistry & Biology. 2011; 18(3):284–91. [PubMed: 21439472]

38. Buas MF, Gu HW, Djukovic D, Zhu JJ, Drescher CW, Urban N, et al. Identification of novel candidate plasma metabolite biomarkers for distinguishing serous ovarian carcinoma and benign serous ovarian tumors. Gynecologic Oncology. 2016; 140(1):138–44. [PubMed: 26521694]
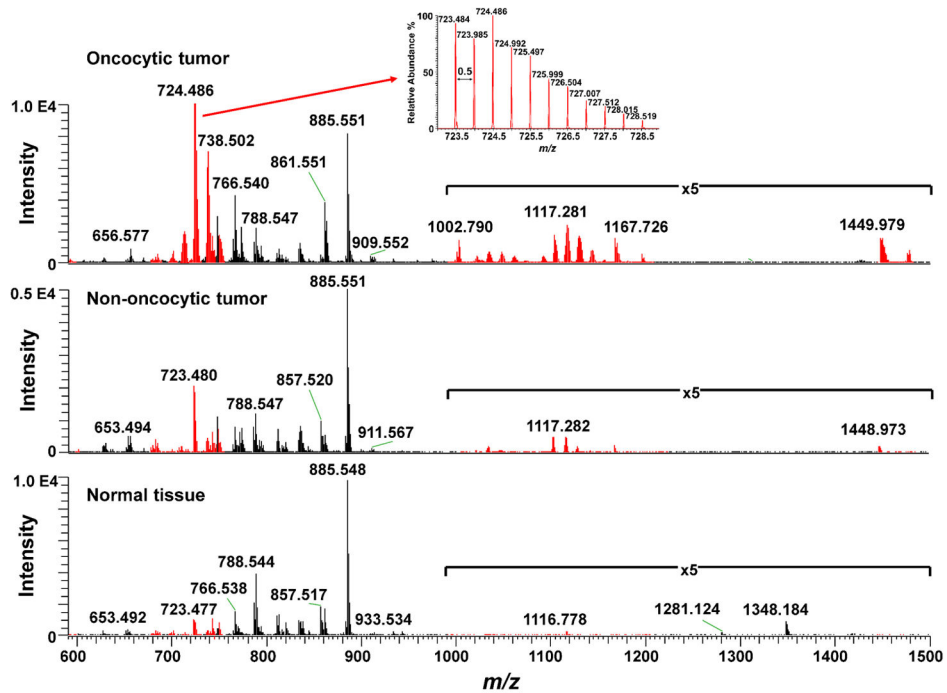
Figure 1. Comparison of DESI-MS results for oncocytic thyroid tumor, non-oncocytic thyroid tumor, and normal thyroid tissues

To aid visualization, representative negative ion mode DESI mass spectra of oncocytic tumor (top) non-oncocytic tumor (middle) and normal thyroid tissue (bottom)mass spectra are shown from *m/z* 590–1500, where CL species (shown in red color) and other GP are detected (for full *m/z* range, please see Supporting Figure 1). Inset in top spectrum shows the mass spectrum of doubly charged CL ion in the mass region from *m/z* 723 to *m/z* 729 with a 0.5 mass difference between each peak (characteristic of doubly charged ions).
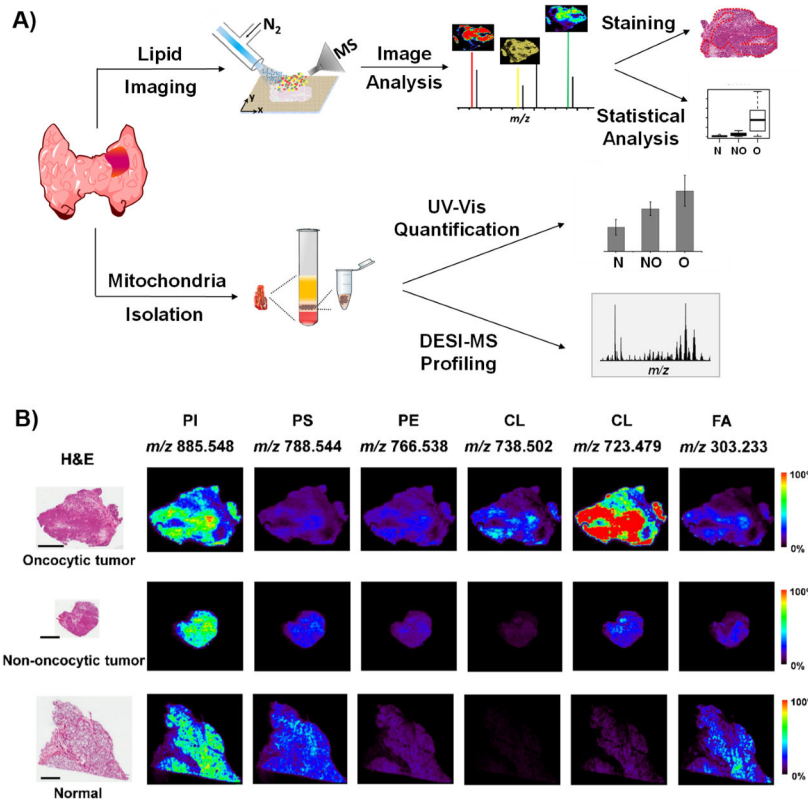
Figure 2. Experimental design for tissue analysis and imaging using DESI-MSI
A) Workflow for imaging and mitochondria isolation experiments in thyroid tissues. **B)** DESI-MSI analysis of an oncocytic tumor, non-oncocytic tumor and normal thyroid tissues. The optical images on the left are from the same tissue sections which were H&E stained after analyzed by non-destructive DESI-MS imaging. Scale bar=4 mm. Six representative ion images from different lipid ions, including PI (20:4/18:0) at *m/z* 885.548, PS (18:1/18:0) at *m/z* 788.544, PE (20:4/18:0) at *m/z* 766.538, CL (20:4/20:2/18:1/16:0 or 20:3/18:2/18:1/18:1 or 20:2/18:2/18:2/18:1) at *m/z* 738.502, CL (18:2/18:2/18:2/18:2 or 20:4/18:2/18:2/16:0) at *m/z* 723.479, and FA (20:4) at *m/z* 303.233 are presented.
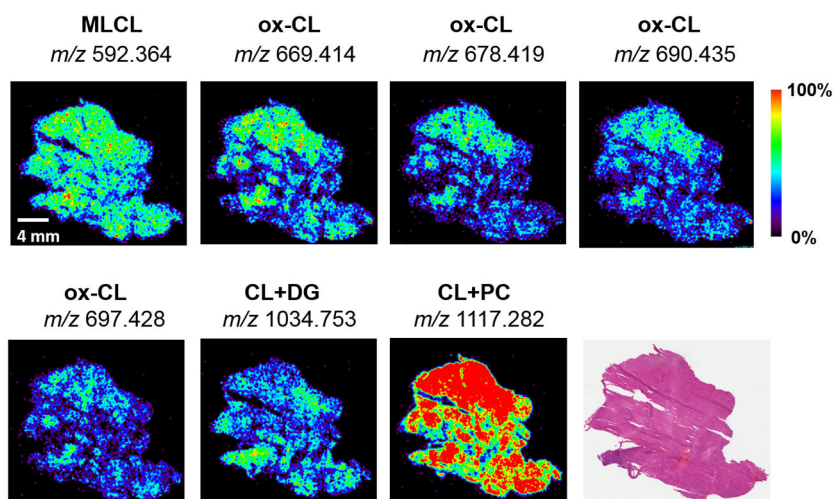
Figure 3. ox-CL, MLCL, and CL+PC and CL+DG ions are observed in regions of tissue samples of oncocytic cells accumulation

DESI-MS images display the spatial distribution of selected CL species in an oncocytic thyroid tumor sample, as well as the optical image of the H&E stained tissue section.
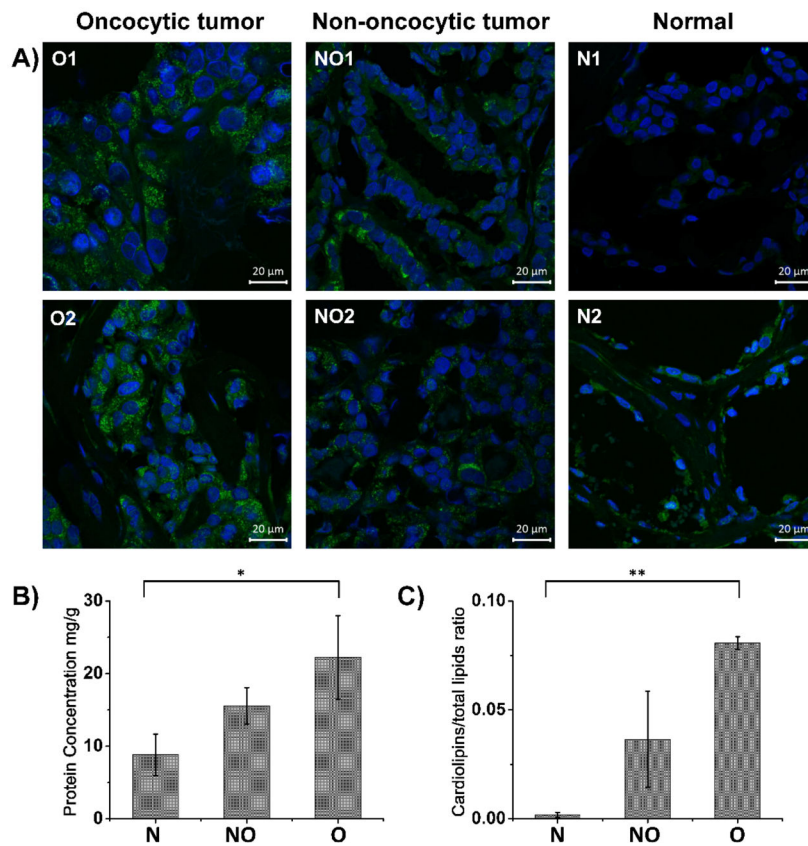
Figure 4. Mitochondria accumulation and changes in mitochondrial CL composition occur in oncocytic tumors

A) Confocal images for oncocytic tumor (O1 and O2), non-oncocytic tumor (NO1 and NO2), and normal (N1 and N2) thyroid tissues. **B)** UV-Vis analysis for protein concentration of mitochondrial isolation from three groups, including normal thyroid tissues, non-oncocytic thyroid tumors, and oncocytic thyroid tumors, (*P<0.001). **C)** Normalized CL intensities of the isolated mitochondria from normal thyroid tissues, non-oncocytic thyroid tumors, and oncocytic thyroid tumors, at the same concentration (3 μg protein/g of tissue) (**P<0.001). P < 0.001 was considered as significant.
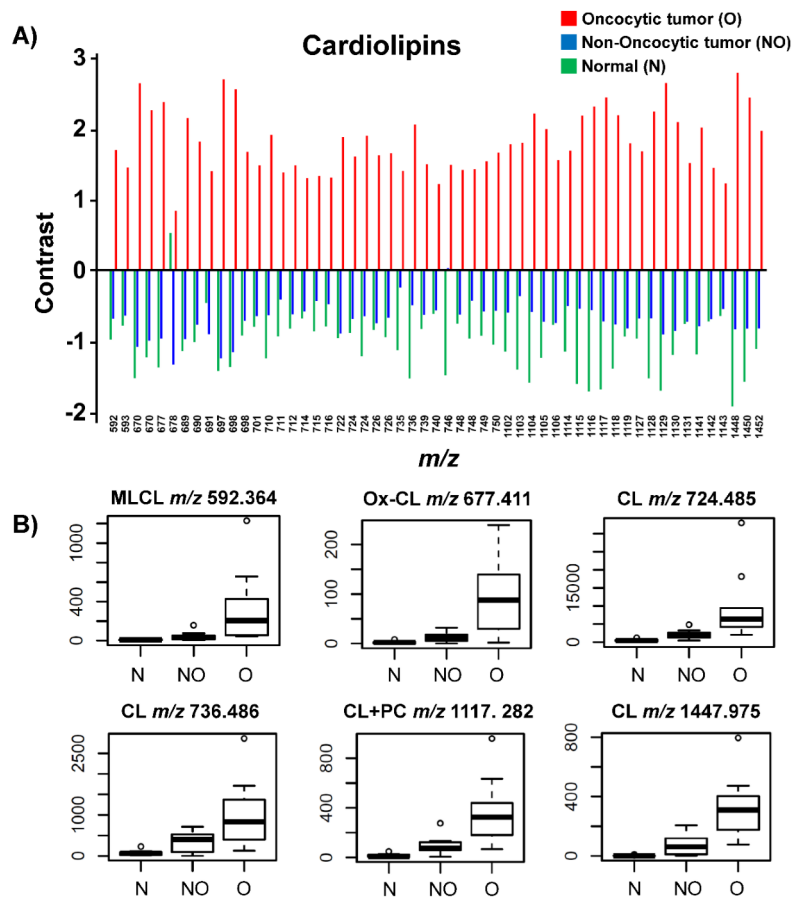
Figure 5. SAM analysis for identifying statistically significant ions (*m/z*) from DESI-MSI data
A) Comparison of contrast values of CLs among oncocytic thyroid tumors, non-oncocytic thyroid tumors, and normal thyroid tissue (n=30). The "contrast value" is the average normalized intensity for that group relative to the overall average intensity. **B)** Box plots show the results obtained using SAM for selected ions including MLCL, ox-CL, CLs, and CL+PC species with FDR=0.

Table 1

Representative CL species identified using high mass resolution/high mass accuracy and tandem mass spectrometry analyses.

Measured m/z	Lipid Class[a]	Tentative Attribution	Exact m/z	Mass Error (ppm)[c]	Proposed Formula
592.3641	MLCL	CL(54:5)	592.3640	0.2	$C_{63}H_{112}O_{16}P_2$
669.4135	ox-CL[b]	20:4/18:2/16:0/9:1(OH)	669.4137	−0.2	$C_{72}H_{126}O_{18}P_2$
677.4108	ox-CL	18:2/18:2/18:2/9:1(OOH)	677.4112	−0.1	$C_{72}H_{126}O_{19}P_2$
678.4187	ox-CL	18:2/18:2/18:1/9:1(OOH)	678.4190	−0.3	$C_{72}H_{128}O_{19}P_2$
689.4292	ox-CL	18:2/18:2/18:2/12:2(OH)	689.4293	−0.2	$C_{75}H_{130}O_{18}P_2$
690.4352	ox-CL	18:2/18:2/18:1/12:2(OH) 20:4/18:1/16:0/12:2(OH)	690.4372	−2.8	$C_{75}H_{132}O_{18}P_2$
697.4279	ox-CL	CL(OO-65:8)	697.4268	1.1	$C_{75}H_{130}O_{19}P_2$
697.4635	CL	18:2/18:2/18:2/14:0 20:2/18:2/16:2/14:0	697.4632	0.5	$C_{77}H_{138}O_{17}P_2$
701.4929	CL	18:1/18:1/18:0/14:0	701.4945	−0.5	$C_{77}H_{146}O_{17}P_2$
706.4869	CL	18:2/18:1/18:1/15:0	706.4867	0.3	$C_{78}H_{144}O_{17}P_2$
710.4709	CL	18:2/18:2/18:2/16:1	710.4710	0.1	$C_{79}H_{140}O_{17}P_2$
723.4789	CL	18:2/18:2/18:2/18:2 20:4/18:2/18:2/16:0	723.4788	0.1	$C_{81}H_{142}O_{17}P_2$
724.4851	CL	18:2/18:2/18:2/18:1 20:2/18:2/18:1/16:2	724.4867	−1.7	$C_{81}H_{144}O_{17}P_2$
732.4821	ox-CL	18:2/18:1/19:1/17:3(OH) 18:4(OH)/18:2/18:1/16:0	730.4841	−2.8	$C_{81}H_{142}O_{18}P_2$
735.4783	CL	20:4/18:2/18:2/18:2	735.4788	−0.7	$C_{83}H_{142}O_{17}P_2$
736.4866	CL	20:4/18:2/18:2/18:1 20:3/18:2/18:2/18:2	736.4867	−0.1	$C_{83}H_{144}O_{17}P_2$
737.4944	CL	20:4/18:2/18:1/18:1 20:3/18:2/18:2/18:1 20:2/18:2/18:2/18:2	737.4945	−0.1	$C_{83}H_{146}O_{17}P_2$
738.5022	CL	20:4/20:2/18:1/16:0 20:3/18:2/18:1/18:1 20:2/18:2/18:2/18:1	738.5023	−0.2	$C_{83}H_{148}O_{17}P_2$
745.4914	ox-CL	CL(O74:8)	745.4910	−0.7	$C_{83}H_{144}O_{18}P_2$
747.4780	CL	22:6/20:4/18:2/16:0	747.4788	−0.8	$C_{85}H_{142}O_{17}P_2$

Measured m/z	Lipid Class[a]	Tentative Attribution	Exact m/z	Mass Error (ppm)[c]	Proposed Formula
1034.7526	**CL+DG**	CL+DG(108:9)	1034.7556	−2.9	$C_{120}H_{216}O_{22}P_2$
1035.7604	**CL+DG**	CL+DG(108:8)	1035.7635	−3.0	$C_{120}H_{218}O_{22}P_2$
1047.7614	**CL+DG**	CL+DG(110:10)	1047.7635	−2.0	$C_{122}H_{220}O_{22}P_2$
1102.2593	**CL+PC**	CL+PC(106:12)	1102.2599	−0.5	$C_{123}H_{222}O_{25}NP_3$
1117.2816	**CL+PC**	CL+PC(108:9)	1117.2834	−1.6	$C_{125}H_{228}O_{25}NP_3$

[a]CL = cardiolipin (X:Y) denotes the total number of carbons and double bonds in the fatty acid chains.

[b]ox-CL =oxidized cardiolipin

[c]Mass errors were calculated based on the exact monoisotopic m/z of the deprotonated form of the assigned molecules.